

Domino Tunneling

Peter R. Schreiner,^{*,1} J. Philipp Wagner,¹ Hans Peter Reisenauer,¹ Dennis Gerbig,¹ David Ley,¹ János Sarka,^{‡,§} Attila G. Császár,^{*,‡,§} Alexander Vaughn,^{||} and Wesley D. Allen^{*,||}

¹Institute of Organic Chemistry, Justus-Liebig University, Heinrich-Buff-Ring 58, D-35392 Giessen, Germany

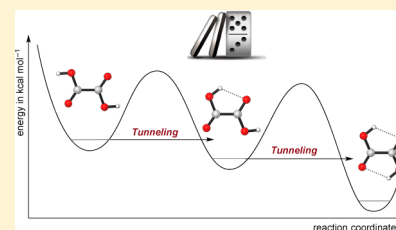
[‡]Laboratory of Molecular Structure and Dynamics, Institute of Chemistry, Eötvös University, PO Box 32, Budapest 112, Hungary, H-1518

[§]MTA-ELTE Complex Chemical Systems Research Group, Eötvös University, Budapest, Pázmány Péter Sétány 1/A, Hungary, H-1117

^{||}Center for Computational Quantum Chemistry and Department of Chemistry, University of Georgia, Athens, Georgia 30602, United States

Supporting Information

ABSTRACT: Matrix-isolation experiments near 3 K and state-of-the-art quantum chemical computations demonstrate that oxalic acid [**1**, (COOH)₂] exhibits a sequential quantum mechanical tunneling phenomenon not previously observed. Intensities of numerous infrared (IR) bands were used to monitor the temporal evolution of the lowest-energy O–H rotamers (**1cTc**, **1cTt**, **1tTt**) of oxalic acid for up to 19 days following near-infrared irradiation of the matrix. The relative energies of these rotamers are 0.0 (**1cTc**), 2.6 (**1cTt**), and 4.0 (**1tTt**) kcal mol⁻¹. A **1tTt** → **1cTt** → **1cTc** isomerization cascade was observed with half-lives (*t*_{1/2}) in different matrix sites ranging from 30 to 360 h, even though the sequential barriers of 9.7 and 10.4 kcal mol⁻¹ are much too high to be surmounted thermally under cryogenic conditions. A general mathematical model was developed for the complex kinetics of a reaction cascade with species in distinct matrix sites. With this model, a precise, global nonlinear least-squares fit was achieved simultaneously on the temporal profiles of nine IR bands of the **1cTc**, **1cTt**, and **1tTt** rotamers. Classes of both fast (*t*_{1/2} = 30–50 h) and slow (*t*_{1/2} > 250 h) matrix sites were revealed, with the decay rate of the former in close agreement with first-principles computations for the conformational tunneling rates of the corresponding isolated molecules. Rigorous kinetic and theoretical analyses thus show that a “domino” tunneling mechanism is at work in these oxalic acid transformations.

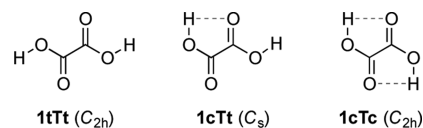


INTRODUCTION

Quantum mechanical tunneling, a classically forbidden process in which a system passes through rather than over an energy barrier,¹ has recently emerged as a control element for chemical reactions.² Such *tunneling control*³ expands the well-known concepts of classical kinetic and thermodynamic control of a reaction by recognizing that product formation may be governed not by the lowest activation barrier or lowest free energy but by the most facile tunneling process.⁴ Here we present experimental observation and theoretical verification of stepwise tunneling that causes isomerization of the low-lying rotational isomers (rotamers) of oxalic acid, at temperatures much too low for thermal reactions.

Oxalic acid (**1**, ethanedioic acid, Scheme 1), the smallest dicarboxylic acid, is a product of biomass degradation and fossil fuel burning. Dicarboxylic acids are common in atmospheric aerosols, with **1** being the most abundant in the troposphere.⁵ Computations⁶ indicate the existence of five or six planar rotamers of **1** and show that an *s-trans* (T) orientation of the carbonyl groups is energetically preferred. Three T rotamers of this type (**1cTc**, **1cTt**, **1tTt**, Scheme 1) exist with different OH orientations, displaying either *s-trans* (t) or *s-cis* (c) H–O–C–C dihedral angles.⁷ In the gas phase^{6c,8} and in noble-gas

Scheme 1. Oxalic Acid (1**) Rotamers (t/c = *s-trans*/*s-cis* H–O–C–C dihedral angle; T = *s-trans* O=C–C=O angle) with Point Group of the Equilibrium Structures in Parentheses^a**



^aThe dashed lines highlight favorable hydrogen-bonding interactions within five-membered rings.

matrices,^{6a,9} **1cTc** is lowest in energy because it exhibits internal hydrogen bonding within favorable five-membered rings.¹⁰ While the **1cTc**^{6a,11} and **1cTt**^{6c} conformers have long been known, **1tTt** was identified unequivocally through matrix-isolation IR spectroscopy only in 2000.^{6b} A tunneling phenomenon has not been reported for the interconversion of the oxalic acid rotamers. While hydrogen tunneling is common, it has become increasingly appreciated in the past few

Received: April 8, 2015

Published: June 1, 2015

years, in particular for determining the rotamerization kinetics of carboxylic acids.^{10,12} Here we uncover a hitherto unreported consecutive hydrogen tunneling conformational interconversion, which we term domino tunneling.

The oxalic acid isomeric structures,^{6a,c,8,9} rotamerizations,^{6a,b,13} and especially unimolecular decomposition¹⁴ have been very well elaborated. In contrast, tunneling processes in **1** have *not* been observed, even though other organic acids display relatively fast rotational isomerizations of hydroxyl groups with inherent tunneling half-lives ranging from 10^{-5} s (benzoic acid derivatives),^{12a} several seconds (acetic acid,^{12j} glycine,^{12c} and alanine¹⁵), to minutes (formic acid^{12q}) at cryogenic temperatures in the matrix. Attempts were made in 2013 to detect tunneling from **1tTt** and **1cTt** under matrix isolation conditions (argon, 19 K) utilizing Raman spectroscopy,¹³ but only within a 3 h time interval; it was argued, based on low levels of theory, that tunneling either does not occur or is very slow. These observations were rationalized by evaluating Wentzel–Kramers–Brillouin (WKB)¹⁶ tunneling rates on the basis of density functional theory (DFT) computations. Here, we present our examination of **1** with more extensive experiments and definitive theory, and we discovered a stepwise, nonclassical rotational isomerization mechanism akin to falling dominos. This term emphasizes our classical view of two independent processes that do not require concertedness or quantum entanglement.

RESULTS AND DISCUSSION

Highly accurate energetics for the three conformers of **1** and their interconnecting transition states (Figure 1) were

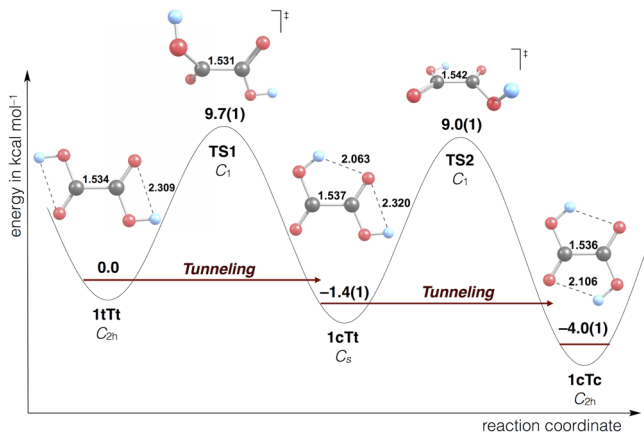


Figure 1. Computed (FPA) potential energy profile for the stepwise interconversion of **1tTt** to **1cTc**. Bond distances given in Å. Numbers in parentheses are uncertainties of the FPA computations.

determined from focal point analyses (FPAs),^{2,17} which entail a hierarchical series of electronic wave function computations designed to converge on the dual complete basis set (CBS) and full electron correlation limit of *ab initio* quantum chemistry. The FPAs executed here employed correlation-consistent Gaussian orbital basis sets¹⁸ as large as augmented quintuple- ζ (aug-cc-pV5Z) and coupled-cluster correlation treatments through the level of quadruple excitations [CCSDT(Q)].¹⁹ Details of the FPA procedures, including optimized reference geometries and convergence tables, are provided in the Supporting Information (SI). Our FPA approach pinpoints energy differences to about $0.1 \text{ kcal mol}^{-1}$,^{2,20} well beyond the

accuracy delivered by previous DFT²¹ or second-order Møller–Plesset perturbation (MP2) computations.^{6a,c,d,13,22}

Our final FPA results place **1cTc** lowest in energy, with **1cTt** next at $2.6(1) \text{ kcal mol}^{-1}$ and **1tTt** third at $4.0(1) \text{ kcal mol}^{-1}$. Referring to Figure 1, these relative energies can be rationalized from the shorter distances and enhanced $\text{H}^{\delta+}\cdots\text{O}^{\delta-}$ electrostatic interactions found in the five-membered rings [$r(\text{H}\cdots\text{O}) = 2.1 \text{ \AA}$] versus the four-membered alternatives [$r(\text{H}\cdots\text{O}) = 2.3 \text{ \AA}$]. Our high-level results rectify a disturbing scatter of relative energies appearing in the literature for lower levels of theory, namely, $1.7\text{--}2.9 \text{ kcal mol}^{-1}$ for **1cTt** and $2.1\text{--}4.7 \text{ kcal mol}^{-1}$ for **1tTt**.^{6a-c,7,13,21} Most importantly, our FPA work yields $9.7(1)$ and $10.4(1) \text{ kcal mol}^{-1}$ for the **1tTt** \rightarrow **1cTt** (TS1) and **1cTt** \rightarrow **1cTc** (TS2) isomerization barriers, respectively, which corrects much higher values of 12.9 (TS1) and $14.8 \text{ kcal mol}^{-1}$ (TS2) reported earlier.^{7,13,21} Because the tunneling probability is proportional to a function of the exponential of the square root of the barrier height,² the tunneling half-life ($t_{1/2}$) of **1** was severely overestimated by the computations in ref 13, which predicted $t_{1/2}$ to be ca. 19 orders of magnitude longer than that of formic acid,^{12q} for which $t_{1/2}$ is a few minutes.

The structural and energetic properties of **1** established here are akin to those of other common α -keto carboxylic acids such as glyoxylic,^{10,23} pyruvic,^{2,10} cyclopropylglyoxylic,¹⁰ and phenylglyoxylic acid²⁴ as well as oxalic acid monoamide.²⁵ Thus, the possibility of conformational tunneling exists, and because **1** bears two carboxylic acid groups, the dynamics may be independent or cooperative. In search of intriguing tunneling phenomena, we probed **1** experimentally with low-temperature matrix isolation techniques.

Oxalic acid was evaporated at a pressure of about 10^{-6} mbar at room temperature and then co-condensed with excess neon at 3 K onto a CsI window. Near infrared (NIR, continuous blackbody irradiation, ca. $0.5\text{--}1.5 \mu\text{m}$) excitation generated higher energy conformers of **1**; IR spectroscopy was then used to identify **1tTt**, **1cTt**, and **1cTc** (Figure 2) and follow their temporal evolution.

Our IR spectra agree well with those determined previously^{6b} in an argon matrix and at a higher temperature (7.5 K). Because

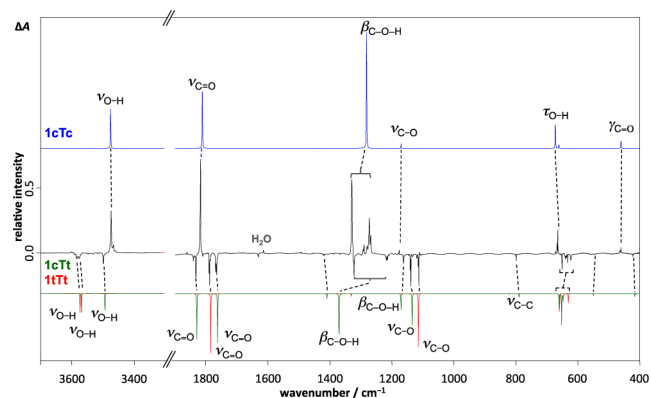


Figure 2. Difference IR spectra of matrix isolated **1** after broad-band NIR irradiation overnight in solid neon at 3 K. Assignments to the three lowest-lying isomers are shown by correspondence to the computed bands plotted up (**1cTc**, blue, decaying) and down (**1cTt**, green; **1tTt**, red, both growing). Vibrational motions are denoted as ν = bond stretch, β = bond angle, γ = out-of-plane angle, and τ = torsion. The computed frequencies include VPT2 anharmonicity corrections, except for the two $\beta_{\text{C-O-H}}$ bands in the Fermi resonance region (see SI).

IR radiation promotes rotamerization of oxalic acid,^{6a} the exposure of the sample to the globar of the IR spectrometer was kept as short as possible. Moreover, a cutoff filter was used that only allows the passage of photon energies below 2200 cm⁻¹ to avoid affecting the relative rotamer populations; the matrix was otherwise kept in the dark at all times. The IR bands of **1cTc**, **1cTt**, and **1tTt** were assigned through matching with vibrational frequencies computed at a high level of electronic structure theory (SI); harmonic frequencies (ω_i) were obtained using the coupled-cluster CCSD(T) method²⁶ with a correlation-consistent aug-cc-pVTZ basis set,^{18c} while anharmonic corrections ($\nu_i - \omega_i$) were determined at the B3LYP/6-311++G(d,p) level²⁷ via the second-order vibrational perturbation theory (VPT2) approach.²⁸

In contrast to an earlier report,¹³ we *did* observe a “dark process” after excitation of matrix isolated **1** with NIR irradiation (cf. Figure S3). The signals of the higher-lying isomers **1tTt** and **1cTt** disappeared over time with a concomitant increase of the vibrational intensities of **1cTc**. Because both isomerization barriers are around 10 kcal mol⁻¹, classical over-the-barrier reactions are not possible, as these would first become significant only at about 120 K. We conclude that the system is driven into the **1cTc** potential energy minimum via tunneling rotamerization at 3 K in order to achieve thermodynamic equilibrium. The observed conformational tunneling was very slow and required measurements for up to 19 days; this is very likely the reason why it remained undetected in earlier studies (*vide supra*).¹³

A quantitative description of the kinetics of relaxation of matrix-isolated **1** after NIR irradiation presents a formidable challenge.²⁹ The excitation process produces a photostationary equilibrium mixture of the **1cTc**, **1cTt**, and **1tTt** conformers whose proportions are unknown because the extinction coefficients of the rotamers are unknown. The **1cTt** species can subsequently be produced from **1tTt** but consumed by decay to **1cTc**. Finally, the possibility exists that each conformer can be trapped in multiple matrix sites with significantly different reaction rates; such behavior is common^{12b,n,q} and is usually described by a coarse dispersive kinetics approach employing simple, phenomenological rate laws.³⁰ In brief, there are various reasons to expect inherent multiexponential character in the relaxation kinetics of **1**, as confirmed by the IR spectral signatures we recorded.

In order to gain maximum information and insight about conformational tunneling in **1**, the experimental data were analyzed using a rigorous and general kinetic model we developed to properly account for the essential physical effects. An overview of this model is provided here, while a more complete description is given in the SI. Consider a reaction cascade of n chemical species $A_1 \rightarrow A_2 \rightarrow \dots \rightarrow A_n$ in which the i th species has m_i possible matrix sites to occupy. The differential equation for the population of species A_i in site j_i is

$$\frac{d[A_{i,j_i}]}{dt} = -k_{i,j_i}[A_{i,j_i}] + \sum_{j_{i-1}} p_{(i-1,j_{i-1}) \rightarrow (i,j_i)} k_{i-1,j_{i-1}} [A_{i-1,j_{i-1}}] \quad (1)$$

where k_{i,j_i} is the overall first-order rate constant for the loss of A_{i,j_i} and $p_{(i-1,j_{i-1}) \rightarrow (i,j_i)}$ is the probability that decay of species A_{i-1} in site j_{i-1} to species A_i will populate site j_i . The system of differential equations for the reaction cascade can be solved

analytically. If species A_3 is the end of the cascade, then the total populations in all sites as a function of time are given by

$$[A_1] = [A_1]_0 \sum_{j_1}^{m_1} f_{1,j_1}^0 \exp(-k_{1,j_1} t) \quad (2)$$

$$[A_2] = [A_2]_0 \sum_{j_2}^{m_2} f_{2,j_2}^0 \exp(-k_{2,j_2} t) + [A_1]_0 \sum_{j_1}^{m_1} f_{1,j_1}^0 k_{1,j_1} \sum_{j_2}^{m_2} \frac{p_{(1,j_1) \rightarrow (2,j_2)}}{(k_{2,j_2} - k_{1,j_1})} (\exp(-k_{1,j_1} t) - \exp(-k_{2,j_2} t)) \quad (3)$$

and

$$[A_3] = [A_1]_0 + [A_2]_0 + [A_3]_0 - [A_2]_0 \sum_{j_2}^{m_2} f_{2,j_2}^0 \exp(-k_{2,j_2} t) - [A_1]_0 \sum_{j_1}^{m_1} f_{1,j_1}^0 \sum_{j_2}^{m_2} \frac{p_{(1,j_1) \rightarrow (2,j_2)}}{(k_{2,j_2} - k_{1,j_1})} (k_{2,j_2} \exp(-k_{1,j_1} t) - k_{1,j_1} \exp(-k_{2,j_2} t)) \quad (4)$$

where $f_{i,j_i}^0 = [A_{i,j_i}]_0/[A_i]_0$ is the initial fractional occupation of species i in site j_i .

A nonlinear least-squares fit to eqs 2–4 was performed on the kinetic data measured from nine matrix-isolation IR bands: **1tTt** (1783–1793, 1107–1117) cm⁻¹, **1cTt** (1827–1836, 1760–1773, 1211–1223, 1135–1144) cm⁻¹, and **1cTc** (1813–1825, 1260–1285, 1318–1337) cm⁻¹. The spectral data were measured over 460 h, and a total of 108 data points were compiled. Band intensities were determined by numerical integration over the ranges given above. Baselines were set by the absorptions at the end points of the ranges. Some overlapping, contaminating peaks change with respect to time in the opposite direction as the target peaks. In these cases deconvolution was performed by fitting the overall band profiles to combinations of Gaussians and/or hyperbolic secant functions; the contributions from functions describing the contaminants were then subtracted from the integrated band intensities.

The slow components of the bands make it impossible to follow the decay long enough to reach the asymptotes. Moreover, the area under each band will not decay to zero at infinite time if constant absorptions from contaminants are present and/or some oxalic acid molecules are trapped in sites that preclude tunneling. Therefore, the measured intensity $I_{ij}(t)$ of each band j of species i was reduced by a time-independent shift s_{ij} before execution of the fits. These shifts were determined by minimizing the quantity:

$$S_i = \sum_{j < k} \sum_m \left(\frac{I_{i,j}(t_m) - s_{i,j}}{I_{i,j}(0) - s_{i,j}} - \frac{I_{i,k}(t_m) - s_{i,k}}{I_{i,k}(0) - s_{i,k}} \right)^2 \quad (5)$$

where the sums run over all times t_m and pairs of bands (j,k) for which measurements were made for species i . This approach produced remarkable consistency among the kinetic data from the various bands of each conformer and yielded optimized s_{ij} parameters in full accord with visual inspection of the decay and purity of the bands.

Preliminary fits of the IR bands for **1tTt** alone showed that the decay is indisputably multiexponential. Satisfactory fits of

the **1tTt** data within the experimental error bars were achieved by assuming only two classes of matrix sites with distinct rate constants $k_{1,1}$ (slow) and $k_{1,2}$ (fast). Including phenomenological slow and fast sites to derive a kinetic model for tunneling reactions under matrix isolation conditions has been shown to be a reasonable approach to this difficult kinetic picture.³¹ Including a third class merely gave an optimized rate constant $k_{1,3} = 0$, which is equivalent to a baseline shift. The domino kinetic equations also require the time evolution of the **1cTt** bands to be multiexponential, despite the fact that the **1cTt** data can be fit rather well with a single, phenomenological rate constant. For consistency, we adopted two classes of sites for both the **1tTt** and **1cTt** conformers in the final kinetic analysis. The kinetic equations are independent of the number of **1cTc** classes.

Alternative exploratory fits of the **1tTt** bands were executed on the basis of eq 2 with the $f_{1,j}^0$ quantity replaced by a smooth distribution function over a continuum of sites. Accordingly, we tested the form:

$$\frac{[A_1]}{[A_1]_0} = \int_0^{k_{\max}} f_1(k) \exp(-kt) dk \quad (6)$$

where k_{\max} is the maximum rate constant possible for the continuum of sites. The distribution function $f_1(k)$ was represented as a normalized cubic function of k and constrained to zero at the origin. With this form of $f_1(k)$, the integration in eq 6 was performed analytically to obtain a three-parameter function describing the time evolution of the **1tTt** bands. Nonlinear least-squares fits were then executed, but the quality of the fits was not satisfactory. In brief, we found that eq 6 with a broad distribution function is much inferior to eq 2 in fitting the observed IR bands of **1tTt**. The oxalic acid matrix-isolation spectra appear to be described better by sharper distribution functions with two peaks rather than broad, featureless $f_1(k)$ functions arising from strongly dispersive kinetics. Nevertheless, we do not claim that our fitting model applied to the limited number of observed bands represents the full physical picture present in the matrix.

The final kinetic fit employed four ($\tau_{1,1}$, $\tau_{1,2}$, $\tau_{2,1}$, $\tau_{2,2}$) half-lives corresponding to the rate constants ($k_{1,1}$, $k_{1,2}$, $k_{2,1}$, $k_{2,2}$), along with four population ratios: $\gamma_1 = [\mathbf{1tTt}]_0/[\mathbf{1cTt}]_0$, $\gamma_2 = [\mathbf{1cTt}]_0/[\mathbf{1cTc}]_0$, $\beta_1 = [\mathbf{1tTt}]_{2,0}/[\mathbf{1tTt}]_{1,0}$, and $\beta_2 = [\mathbf{1cTt}]_{2,0}/[\mathbf{1cTt}]_{1,0}$. The β parameters represent the initial occupation ratios of class 2 (fast) to class 1 (slow) matrix sites. A global nonlinear least-squares fit was executed simultaneously on all nine IR bands arising from the three conformers, as detailed in the SI. The quality of the fit is excellent, as shown in Figure 3.

To summarize the experimental findings, the **1tTt** conformer exhibits the half-lives ($\tau_{1,1}$, $\tau_{1,2}$) = (355 ± 18 h, 43 ± 4 h) in the (slow, fast) sites and $\beta_1 = 0.41 \pm 0.05$ as the initial fast:slow population ratio (1 σ error bars). For **1cTt** the corresponding parameters are ($\tau_{2,1}$, $\tau_{2,2}$) = (260 ± 30 h, 30 ± 20 h) and $\beta_2 = 0.09 \pm 0.07$. The species total population ratios from the fit were $\gamma_1 = 0.35 \pm 0.05$ and $\gamma_2 = 0.68 \pm 0.03$, which correspond to the initial mole fractions ($X_{\mathbf{1tTv}}$, $X_{\mathbf{1cTv}}$, $X_{\mathbf{1cTc}}$) = (0.13, 0.35, 0.52). These mole fractions are in remarkable agreement with the corresponding values ($X_{\mathbf{1tTv}}$, $X_{\mathbf{1cTv}}$, $X_{\mathbf{1cTc}}$) = (0.14, 0.32, 0.54) obtained by measuring the initial signals of the carbonyl stretching bands and converting them to population ratios using IR intensities computed from the CCSD(T)/aug-cc-pVTZ level of theory.^{18c,26}

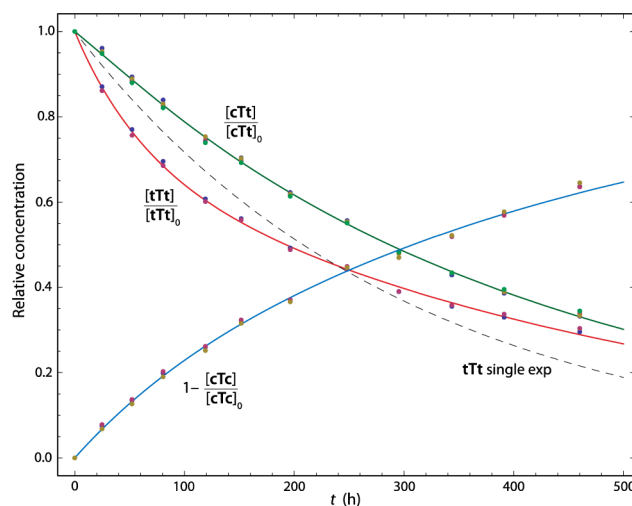


Figure 3. Time evolution of oxalic acid conformer concentrations after NIR irradiation of the matrix. Color-coded curves (same colors as in Figure 2: **1cTc**, blue; **1cTt**, green; **1tTt**, red) show the global, nonlinear least-squares fit of the kinetic model to the matrix-isolation IR data (**1tTt**, **1cTt**, **1cTc**). The dashed curve is the best possible single-exponential fit for **1tTt**; 108 independent data points are shown.

Figure 4 illustrates the time evolution of the conformer populations. At $t = 0$, **1tTt** and **1cTt** are generated from **1cTc**

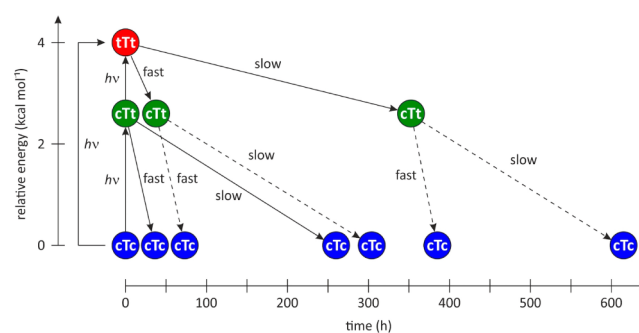


Figure 4. Illustration of the relaxation of isomers of **1** over time via tunneling from phenomenologically fast and slow matrix sites. The time increments for the downward arrows are the corresponding experimental tunneling half-lives: **1tTt** (slow, fast) = (43, 355) h and **1cTt** (slow, fast) = (30, 260) h. The (solid, dashed) lines represent (first, second) steps of decay.

through NIR irradiation, populating different matrix sites whose decay rates can be grouped into fast and slow classes (the simplest reliable model corresponding to the available experimental results). The initial **1cTt** in fast sites tunnels to **1cTc** with a half-life $\tau_{2,2} = 30$ h, and the production of **1cTc** persists as slow **1cTt** decays with a time scale of $\tau_{2,1} = 260$ h. However, **1cTt** reforms from the isomerization of the initial fast **1tTt** that occurs with $\tau_{1,2} = 43$ h, and this replenishment continues for a long time as slow **1tTt** decays with a half-life $\tau_{1,1} = 355$ h. Nonetheless, these sources are not sufficiently fast to prevent the concentration of **1cTt** from falling continuously with time, as shown in Figure 3. In addition to formation in a single step from the initial **1cTt**, the **1cTc** isomer continues to appear from the secondary processes depicted by dashed lines in Figure 4.

The theoretical basis for the observed relaxation kinetics was established by computing tunneling rates for both the **1tTt** →

1cTt and **1cTt** → **1cTc** isomerizations. The MP2/aug-cc-pVTZ method was employed to map out the associated intrinsic reaction paths (IRPs)³² and to determine zero-point vibrational energies (ZPVEs) for all orthogonal modes at each point along these steepest-descent routes.³³ Final vibrationally adiabatic potential energy curves along the IRPs were then constructed from high-quality all-electron (AE) CCSD(T)/aug-cc-pwCVTZ energy points^{18d,26} appended with the ZPVEs. Tunneling probabilities (κ) for barrier collisions were computed using an exact numerical integration procedure described in the SI as well as the semiclassical WKB method.¹⁶

The reaction modes of **1tTt** and **1cTt** that lead to **TS1** and **TS2** have harmonic vibrational frequencies (ω_0) of 627 and 658 cm^{-1} , respectively. Conformational tunneling rates were computed as the product of the tunneling probability (κ) and the classical rate (ω_0) at which the reactant hits the barrier, adopting the reaction-mode ZPVE of $\omega_0/2$ as the energy (ϵ) of the barrier collisions under cryogenic conditions. This first-principles approach has proved very effective for computing deep tunneling rates in numerous systems,^{2,12a,20,24,34} as it seemingly provides a good cancellation of multidimensional coupling and reaction path curvature effects. Naturally, high levels of electronic structure theory must be employed as tunneling rates are sensitive to even small energetic differences. Multiplicative factors were included in the reaction rates to account for the two-fold degeneracy of the tunneling path (above and below the molecular plane) for both **1tTt** and **1cTt** as well as the presence of two acid groups exhibiting tunneling in the **1tTt** case.

The exact integration and WKB methods yield the half-lives ($\tau_{\text{exact}}, \tau_{\text{WKB}}$) = (40, 44) h for the first isomerization **1tTt** → **1cTt**, whereas ($\tau_{\text{exact}}, \tau_{\text{WKB}}$) = (21, 26) h are obtained for the somewhat faster second step **1cTt** → **1cTc**. These theoretical gas-phase values are in excellent agreement with the experimental half-lives (43 ± 4 h, 30 ± 20 h) reported above for the fast (**1tTt**, **1cTt**) matrix sites. Hence, the observed fast tunneling processes appear largely unaffected by the matrix environment, whereas tunneling in the slow sites is hindered by interactions with the surrounding matrix. This occurrence is not surprising, because site-dependent reaction rates are well-known in matrix isolation experiments (*vide supra*).^{12g} In this regard it must be emphasized that increases of only 5% and 0.7 kcal mol^{-1} in the width and height of the barriers, respectively, are sufficient to explain the observed differences in the fast and slow half-lives of **1tTt** and **1cTt**. It is not difficult to envision how such changes could be caused by interference of the matrix atoms in the sweeping torsional motions involved in the isomerizations.

In our experiments the IR signatures of the slow and fast sites of **1** cannot be cleanly resolved. Furthermore, some bands indicate at least six spectroscopically distinguishable matrix sites. For any particular site, however, perturbation of a spectral band does not necessarily imply a significant alteration of the tunneling rate, and *vice versa*. In brief, the recorded matrix-isolation spectra of **1** do not provide an enumeration of all sites with distinct tunneling rates. The kinetic analysis above shows that the measured data can be fully reproduced by the minimal assumption that the tunneling rates fall into only two phenomenological classes, with the fast processes being in exceptional accord with the theoretical rates for tunneling in the gas phase. The appearance of much slower sites clearly shows that conformational tunneling can be affected signifi-

cantly by the environment, a realization that is the first step in understanding how to control tunneling processes further.

The oxalic acid isomerizations completely shut down upon dideuteration of **1**, providing additional evidence of the conformational tunneling mechanism. The d_2 -**1** isotopologue was prepared by repetitive dissolution of **1** in D_2O and subsequent evaporation of the solvent under reduced pressure. A matrix charged with d_2 -**1** was prepared analogously to **1** (for spectral data see Figure S4); some inevitable H/D exchange occurred when samples of d_2 -**1** hit the walls of the matrix apparatus, and thus the sample contained small amounts of monodeuterated d_1 -**1**. NIR broadband excitation was considerably less effective for d_2 -**1** as compared to **1** but sufficient to generate the higher-lying isomers. Once these deuterated species formed, their populations remained unchanged over a time span of at least 3 days, consistent with the computed half-lives of d_2 -**1tTt** and d_2 -**1cTt**, which are of the order of 10^{10} and 10^9 h, respectively.

Cooperative tunneling involving simultaneous rotations about both C–O bonds can be ruled out as a mechanism for the observed isomerizations. We located a second-order saddle point that directly connects **1tTt** with **1cTc**, as characterized in Figure S10. The relative energy of this stationary structure is about twice as high as the **TS1** and **TS2** transition states. Together with the increased effective mass for simultaneous hydrogen torsional motions, the associated energy barrier precludes a direct **1tTt** → **1cTc** transformation via tunneling under cryogenic conditions.

CONCLUSIONS

We demonstrate that the higher-energy rotamers of **1**, similarly to other organic acids, undergo a (relatively slow) tunneling rotamerization, even at 3 K in solid Ne. Indeed, two independent tunneling processes interconvert the higher-lying rotamers of **1** to the minimum structure, a finding which we term domino tunneling.

We developed a general kinetic model to explain the temporal evolution of numerous experimental infrared bands as a tool to deconvolute the experimental spectra acquired over long time periods (up to 19 d). Our phenomenological model based on only two classes of matrix sites (slow, fast) provides just as good a description of domino tunneling in **1** as multistate models or dispersive kinetics. The fast tunneling half-lives are in excellent agreement with those determined from high-level quantum chemical computations in the gas phase. The long half-lives also imply that tunneling sensitively depends on the environment (and therefore can in principle be controlled externally), an observation that was made before^{12d,e,g,k,q} and that is being explored further in various laboratories.

The observed domino tunneling exemplifies the principles of tunneling control,² as the **1cTt** → **1cTc** isomerization is considerably faster than its **1tTt** → **1cTt** counterpart, even though the barrier for the former (**TS2**) is 0.8 kcal mol^{-1} larger than for the latter (**TS1**). Given the chemical similarities in the bond rotations, the difference in the two isomerization rates is rather remarkable. Our experiments demonstrate that tunneling prefers the process with the higher but narrower barrier.^{2,35} In contrast, classical kinetic control based on thermal over-the-barrier processes would require the **1cTt** → **1cTc** isomerization to be the slower one by orders of magnitude at the temperature (3 K) of our experiments.

Oxalic acid also is a ketocarboxylic acid and is thus naturally related to amino acids through (enzymatically facile) reductive amination. Although not generally appreciated, the conformations of α -ketocarboxylic^{23,34} and amino acids^{12c,15,17c,29b,c} are rather similar because only the Lewis-basic keto and amino groups differ in these compounds. The current work on oxalic acid makes it clear that rapid equilibration through tunneling must be taken into account in spectroscopic searches for the plethora of uncharacterized conformers of both α -keto- and, by analogy, amino acids. Indeed, the very question of how many conformers are viable chemical species must now be investigated in light of possible tunneling cascades that can exist in these systems. Such studies are ongoing in our laboratories.

EXPERIMENTAL SECTION

Matrix Isolation Experiments. For the preparation of the matrix samples, **1** was evaporated from a vessel at a pressure of about 10^{-6} mbar at room temperature. The gaseous sample was co-condensed with an excess of neon on a cold CsI window, which was cooled to 3 K with a closed cycle helium cryostat (SHI-4R). Higher energy isomers of **1** were generated by NIR excitation, which was achieved by irradiation with a mercury high-pressure lamp (HBO 200 Osram) in combination with an RG850 long-pass filter (Schott). The IR spectra ($4000\text{--}400\text{ cm}^{-1}$) were recorded on a Bruker VERTEX 70 IR spectrometer. Spectra were taken at a resolution of 0.7 cm^{-1} and were obtained by adding up to 50 interferograms. A LOT Oriel, 4.50 ILP-25 filter was used to cut off all radiation below $4.5\text{ }\mu\text{m}$.

Deuteration. Dideuterated oxalic acid d_2 -**1** was prepared by dissolution of **1** in D_2O and subsequent evaporation of the solvent under reduced pressure; the process was repeated several times. After the final deuteration procedure, crystal water was removed by applying a vacuum for several hours. The vessel from which the solid sample was evaporated to prepare the matrix was flashed with D_2O to reduce the probability of D/H exchange.

Computations. Most of the electronic structure computations utilized single-reference coupled-cluster theory with singles and doubles (CCSD) and a perturbative accounting of triple excitations [CCSD(T)].²⁶ The symbol AE denotes the correlation of all electrons; otherwise, the carbon and oxygen 1s core orbitals were frozen in the computations. The correlation-consistent cc-pVXZ, aug-cc-pVXZ, and aug-cc-pwCVXZ series of basis sets¹⁸ were employed to provide a consistent approach to the complete basis set limit. Final stationary points on the potential energy hypersurface of **1** were optimized at the AE-CCSD(T)/aug-cc-pwCVTZ level of theory with the CFOUR program.³⁶ Companion structures as well as harmonic vibrational frequencies and intensities were obtained with the CCSD(T)/cc-pVTZ and CCSD(T)/aug-cc-pVTZ methods and the same program. The Gamess³⁷ package was used to map out the IRPs, and final single-point energies were determined with MOLPRO.³⁸ Details of the focal-point analyses (FPAs) and the final potential energy curves along the IRPs are given in the SI.

ASSOCIATED CONTENT

Supporting Information

Detailed kinetics of domino tunneling, experimental and theoretical IR bands of **1**, additional experimental IR spectra, tunneling computations and procedures, XYZ-coordinates, absolute energies of all optimized structures, internal coordinates, and focal point energies of all species. The Supporting Information is available free of charge on the ACS Publications website at DOI: 10.1021/jacs.5b03322.

AUTHOR INFORMATION

Corresponding Authors

*prs@org.chemie.uni-giessen.de

*csaszar@chem.elte.hu

*wdallen@uga.edu

Notes

The authors declare no competing financial interest.

ACKNOWLEDGMENTS

This work was primarily supported by an International Collaboration in Chemistry grant from the U.S. National Science Foundation (CHE-1124885) and the Deutsche Forschungsgemeinschaft (Schr 597/18-1) to W.D.A. and P.R.S. An ERA-Chemistry grant supported the collaboration of A.G.C. and P.R.S.; J.S. and A.G.C. thank the Hungarian Scientific Research Fund (OTKA NK83583) for support. J.P.W. is grateful to the Fonds der Chemischen Industrie for a fellowship.

REFERENCES

- (1) Bell, R. P. *Tunnel Effect in Chemistry*; Chapman and Hall: London, 1980.
- (2) Schreiner, P. R.; Reisenauer, H. P.; Ley, D.; Gerbig, D.; Wu, C.-H.; Allen, W. D. *Science* **2011**, *332*, 1300.
- (3) Ley, D.; Gerbig, D.; Schreiner, P. R. *Org. Biomol. Chem.* **2012**, *19*, 3769.
- (4) Patureau, F. W. *Angew. Chem., Int. Ed.* **2012**, *51*, 4784.
- (5) Sorooshian, A.; Varutbangkul, V.; Brechtel, F. J.; Ervens, B.; Feingold, G.; Bahreini, R.; Murphy, S. M.; Holloway, J. S.; Atlas, E. L.; Buzorius, G.; Jonsson, H.; Flagan, R. C.; Seinfeld, J. H. *J. Geophys. Res.* **2006**, *111*, D23S45.
- (6) (a) Nieminen, J.; Räsänen, M.; Murto, J. *J. Phys. Chem.* **1992**, *96*, 5303. (b) Maçôas, E. M. S.; Fausto, R.; Pettersson, M.; Khriachtchev, L.; Räsänen, M. *J. Phys. Chem. A* **2000**, *104*, 6956. (c) Godfrey, P. D.; Mirabella, M. J.; Brown, R. D. *J. Phys. Chem. A* **2000**, *104*, 258.
- (d) Chen, C.; Shyu, S.-F. *Int. J. Quantum Chem.* **2000**, *76*, 541.
- (7) This nomenclature is formally incorrect as *cis* and *trans* must refer to the same substituents; otherwise the *E* and *Z* nomenclature must be employed. In this case the isomers should correctly be termed 1ZTZ, 1ZTE, and 1ETE (in the same order as depicted in Scheme 1). We use the *c/t* nomenclature to avoid confusion with earlier studies.
- (8) Stace, B. C.; Oralaratmanee, C. *J. Mol. Struct.* **1973**, *18*, 339.
- (9) Redington, R. L.; Redington, T. E. *J. Mol. Struct.* **1978**, *48*, 165.
- (10) Gerbig, D.; Schreiner, P. R. *J. Phys. Chem. B* **2014**, *119*, 693.
- (11) Cyvin, S. J.; Alheim, I. *Acta Chem. Scand.* **1970**, *24*, 2648.
- (12) (a) Amiri, S.; Reisenauer, H. P.; Schreiner, P. R. *J. Am. Chem. Soc.* **2010**, *132*, 15902. (b) Bazsó, G.; Góbi, S.; Tarczay, G. *J. Phys. Chem. A* **2012**, *116*, 4823. (c) Bazsó, G.; Magyarfalvi, G.; Tarczay, G. *J. Phys. Chem. A* **2012**, *116*, 10539. (d) Domanskaya, A.; Marushkevich, K.; Khriachtchev, L.; Räsänen, M. *J. Chem. Phys.* **2009**, *130*, 154509. (e) Halasa, A.; Lapinski, L.; Reva, I.; Rostkowska, H.; Fausto, R.; Nowak, M. *J. Phys. Chem. A* **2015**, *119*, 1037. (f) Lamberson, C. R.; Xu, L.; Muchalski, H.; Montenegro-Burke, J. R.; Shmanai, V. V.; Bekish, A. V.; McLean, J. A.; Clarke, C. F.; Shchepinov, M. S.; Porter, N. A. *J. Am. Chem. Soc.* **2013**, *136*, 838. (g) Lopes, S.; Domanskaya, A. V.; Fausto, R.; Räsänen, M.; Khriachtchev, L. *J. Chem. Phys.* **2010**, *133*, 144507. (h) Luckhaus, D. *Phys. Chem. Chem. Phys.* **2010**, *12*, 8357. (i) Mackenzie, R. B.; Dewberry, C. T.; Leopold, K. R. *J. Phys. Chem. A* **2014**, *118*, 7975. (j) Maçôas, E. M. S.; Khriachtchev, L.; Fausto, R.; Räsänen, M. *J. Phys. Chem. A* **2004**, *108*, 3380. (k) Maçôas, E. M. S.; Khriachtchev, L.; Pettersson, M.; Fausto, R.; Räsänen, M. *J. Chem. Phys.* **2004**, *121*, 1331. (l) Maçôas, E. M. S.; Khriachtchev, L.; Pettersson, M.; Fausto, R.; Räsänen, M. *J. Am. Chem. Soc.* **2003**, *125*, 16188. (m) Maçôas, E. M. S.; Khriachtchev, L.; Pettersson, M.; Fausto, R.; Räsänen, M. *J. Phys. Chem. A* **2005**, *109*, 3617. (n) Maçôas, E. M. S.; Khriachtchev, L.; Pettersson, M.; Juselius, J.; Fausto, R.; Räsänen, M. *J. Chem. Phys.* **2003**, *119*, 11765. (o) Maçôas, E. M. S.; Khriachtchev, L.; Pettersson, M.; Lundell, J.; Fausto, R.; Rasanen, M. *Vib. Spec.* **2004**, *34*, 73. (p) Pettersson, M.; Maçôas, E. M. S.; Khriachtchev, L.; Fausto, R.; Räsänen, M. *J. Am. Chem. Soc.* **2003**, *125*,

4058. (q) Pettersson, M.; Maçoãs, E. M. S.; Khriachtchev, L.; Lundell, J.; Fausto, R.; Rasanen, M. *J. Chem. Phys.* **2002**, *117*, 9095.
- (r) Rambaud, C.; Oppenländer, A.; Pierre, M.; Trommsdorff, H. P.; Vial, J.-C. *Chem. Phys.* **1989**, *136*, 335. (s) Tsuge, M.; Khriachtchev, L. *J. Phys. Chem. A* **2014**, *119*, 2628.
- (13) Olbert-Majkut, A.; Ahokas, J.; Pettersson, M.; Lundell, J. *J. Phys. Chem. A* **2013**, *117*, 1492.
- (14) (a) Wobbe, D. E.; Noyes, W. A. *J. Am. Chem. Soc.* **1926**, *48*, 2856. (b) Clark, L. W. *J. Phys. Chem.* **1957**, *61*, 699. (c) Lapidus, G.; Barton, D.; Yankwich, P. E. *J. Phys. Chem.* **1964**, *68*, 1863. (d) Schreiner, P. R.; Reisenauer, H. P. *Angew. Chem., Int. Ed.* **2008**, *47*, 7071. (e) Higgins, J.; Zhou, X. F.; Liu, R. F.; Huang, T. T. S. *J. Phys. Chem. A* **1997**, *101*, 2702.
- (15) (a) Nunes, C. M.; Lapinski, L.; Fausto, R.; Reva, I. *J. Chem. Phys.* **2013**, *138*, 125101/1–12. (b) Bazsó, G.; Najbauer, E. E.; Magyarfalvi, G.; Tarczay, G. *J. Phys. Chem. A* **2013**, *117*, 1952.
- (16) (a) Kramers, H. A. Z. *Phys.* **1926**, *39*, 828. (b) Razavy, M. *Quantum Theory of Tunneling*; World Scientific: Singapore, 2003.
- (17) (a) Császár, A. G.; Allen, W. D.; Schaefer, H. F. *J. Chem. Phys.* **1998**, *108*, 9751. (b) Császár, A. G.; Tarczay, G.; Leininger, M. L.; Polyansky, O. L.; Tennyson, J.; Allen, W. D. Dream or reality: Complete basis set full configuration interaction potential energy hypersurfaces. In *Spectroscopy from Space*; Demaison, J., Sarka, K., Eds.; Kluwer: Dordrecht, 2001; Vol. 20, p 317. (c) Wilke, J. J.; Lind, M. C.; Schaefer, H. F.; Császár, A. G.; Allen, W. D. *J. Chem. Theory Comput.* **2009**, *5*, 1511.
- (18) (a) Dunning, T. H., Jr. *J. Chem. Phys.* **1989**, *90*, 1007. (b) Woon, D. E.; Dunning, T. H., Jr. *J. Chem. Phys.* **1995**, *103*, 4572. (c) Kendall, R. A.; Dunning, T. H., Jr.; Harrison, R. J. *J. Chem. Phys.* **1992**, *96*, 6796. (d) Peterson, K. A.; Dunning, T. H., Jr. *J. Chem. Phys.* **2002**, *117*, 10548.
- (19) (a) Bomble, Y. J.; Stanton, J. F.; Kállay, M.; Gauss, J. *J. Chem. Phys.* **2005**, *123*, 054101. (b) Kállay, M.; Gauss, J. *J. Chem. Phys.* **2005**, *123*, 214105.
- (20) Schreiner, P. R.; Reisenauer, H. P.; Pickard, F. C., IV; Simmonett, A. C.; Allen, W. D.; Mátyus, E.; Császár, A. G. *Nature* **2008**, *453*, 906.
- (21) In attempting to reproduce the B3LYP/aug-cc-pVTZ results of ref 13 with Gaussian 09, we discovered that the ZPVE corrections had been applied incorrectly. The originally reported (**1cTt**, **1fTt**) relative energies of (2.9, 4.7) kcal mol⁻¹ should be (2.5, 4.0) kcal mol⁻¹; likewise, the (**1fTt** → **1cTt**, **1cTt** → **1cTc**) isomerization barriers should be (9.5, 10.4) instead of (12.9, 14.8) kcal mol⁻¹.
- (22) Náhlovská, Z.; Náhlovsky, B.; Strand, T. G. *Acta Chem. Scand.* **1970**, *24*, 2617.
- (23) Olbert-Majkut, A.; Lundell, J.; Wierzejewska, M. *J. Phys. Chem. A* **2013**, *118*, 350.
- (24) Gerbig, D.; Reisenauer, H. P.; Wu, C.-H.; Ley, D.; Allen, W. D.; Schreiner, P. R. *J. Am. Chem. Soc.* **2010**, *132*, 7273.
- (25) Maier, G.; Endres, J.; Reisenauer, H. P. *J. Mol. Struct.* **2012**, *1025*, 2.
- (26) (a) Raghavachari, K.; Trucks, G. W.; Pople, J. A.; Head-Gordon, M. *Chem. Phys. Lett.* **1989**, *157*, 479. (b) Bartlett, R. J.; Watts, J. D.; Kucharski, S. A.; Noga, J. *Chem. Phys. Lett.* **1990**, *165*, 513. (c) Bartlett, R. J.; Watts, J. D.; Kucharski, S. A.; Noga, J. *Chem. Phys. Lett.* **1990**, *167*, 609.
- (27) (a) Lee, C. T.; Yang, W. T.; Parr, R. G. *Phys. Rev. B* **1988**, *37*, 785. (b) Becke, A. D. *Phys. Rev. A* **1988**, *38*, 3098. (c) Krishnan, R.; Binkley, J. S.; Seeger, R.; Pople, J. A. *J. Chem. Phys.* **1980**, *72*, 650. (d) Clark, T.; Chandrasekhar, J.; Spitznagel, G. W.; Schleyer, P. v. R. *J. Comput. Chem.* **1983**, *4*, 294.
- (28) (a) Watson, J. K. G. In *Vibrational Spectra and Structure*; Durig, J. R., Ed.; Elsevier: Amsterdam, 1977; Vol. 6, p 1; (b) Clabo, D. A., Jr.; Allen, W. D.; Remington, R. B.; Yamaguchi, Y.; Schaefer, H. F., III *Chem. Phys.* **1988**, *123*, 187. (c) Simmonett, A. C.; Schaefer, H. F., III; Allen, W. D. *J. Chem. Phys.* **2009**, *130*, 044301.
- (29) (a) Akai, N.; Kudoh, S.; Takayanagi, M.; Nakata, M. *J. Phys. Chem. A* **2002**, *106*, 11029. (b) Lapinski, L.; Nowak, M. J.; Reva, I.; Rostkowska, H.; Fausto, R. *Phys. Chem. Chem. Phys.* **2010**, *12*, 9615.
- (c) Lapinski, L.; Reva, I.; Nowak, M. J.; Fausto, R. *Phys. Chem. Chem. Phys.* **2011**, *13*, 9676. (d) Reva, I.; Nowak, M. J.; Lapinski, L.; Fausto, R. *J. Chem. Phys.* **2012**, *136*.
- (30) (a) Johnson, B. A.; Gamarnik, A.; Garcia-Garibay, M. A. *J. Phys. Chem.* **1996**, *100*, 4697. (b) Johnson, B. A.; Hu, Y.; Houk, K. N.; Garcia-Garibay, M. A. *J. Am. Chem. Soc.* **2001**, *123*, 6941.
- (31) Ertelt, M.; Hrovat, D. A.; Borden, W. T.; Sander, W. *Chem.—Eur. J.* **2014**, *20*, 4713.
- (32) (a) Fukui, K. *J. Phys. Chem.* **1970**, *74*, 4161. (b) Gonzalez, C.; Schlegel, H. B. *J. Chem. Phys.* **1989**, *90*, 2154.
- (33) Allen, W. D.; Bodi, A.; Szalay, V.; Császár, A. G. *J. Chem. Phys.* **2006**, *124*, 224310.
- (34) Gerbig, D.; Schreiner, P. R. *J. Phys. Chem. B* **2014**, *119*, 693.
- (35) (a) Carpenter, B. K. *J. Am. Chem. Soc.* **1983**, *105*, 1700. (b) Kozuch, S.; Zhang, X.; Hrovat, D. A.; Borden, W. T. *J. Am. Chem. Soc.* **2013**, *135*, 17274.
- (36) Stanton, J. F.; Gauss, J.; Harding, M. E.; Szalay, P. G.; with contributions from Auer, A. A., Bartlett, R. J., Benedikt, U., Berger, C., Bernholdt, D. E., Bomble, Y. J., Christiansen, O., Heckert, M., Heun, O., Huber, C., Jagau, T.-C., Jonsson, D., Jusélius, J., Klein, K., Lauderdale, W. J., Matthews, D. A., Metzroth, T., O'Neill, D. P., Price, D. R., Prochnow, E., Ruud, K., Schifmann, F., Stopkowicz, S., Vázquez, J., Wang, F., Watts, J. D. *CFour, Coupled-Cluster techniques for Computational Chemistry, a quantum chemical program package*, 2015 and the integral packages MOLECULE (Almlöf, J. and Taylor, P. R.), PROPS (Taylor, P. R.), ABACUS (Helgaker, T., Jensen, H. J. Aa., Jørgensen, P. and Olsen, J.), and ECP routines by Mitin, A. V. and van Wüllen, C., Austin, TX (USA) and Mainz (Germany).
- (37) Schmidt, M. W.; Baldrige, K. K.; Boatz, J. A.; Elbert, S. T.; Gordon, M. S.; Jensen, J. H.; Koseki, S.; Matsunaga, N.; Nguyen, K. A.; Su, S. J.; Windus, T. L.; Dupuis, M.; Montgomery, J. A. *J. Comput. Chem.* **1993**, *14*, 1347.
- (38) Werner, H. J.; Knowles, P. J.; Knizia, G.; Manby, F. R.; Schütz, M. *WIREs Comput. Mol. Sci.* **2012**, *2*, 242.